Graphene Defects

DOI: 10.1002/anie.200907347

Carbon Spiral Helix: A Nanoarchitecture Derived from Monovacancy Defects in Graphene**

Xingfa Gao, Lili Liu, Stephan Irle, and Shigeru Nagase**

Graphene has diverse applications in molecular electronics due to its unique electronic, thermal, and mechanical properties.[1] Lattice imperfections are introduced into graphene unavoidably during graphene growth or when a graphene sheet is irradiated with high-energy particles.[2] These structural defects are known to significantly affect electronic and chemical properties.[2a,3] A comprehensive understanding of graphene defects is thus of critical importance. In particular, the monovacancy defect has attracted great attention due to its fundamental nature.[4] Recent studies have established that monovacancies exist in graphene as a planar 5/9 isomer with lowered symmetry. The 5/9 isomer is generated by formation of an elongated carbon–carbon bridge across the hole that results from removal of a single carbon atom, which leads to fusion of a five- and a nine-membered ring (Figure 1b).[4] Each 5/9 isomer contributes an intrinsic magnetic moment of about 1 μ_B.[4] Here we report that the stability and therefore electronic structure of the monovacancy defect is determined by the distance from the graphene periphery: The magnetic, planar 5/9 isomer is most stable in the center of graphene flakes, whereas the nonmagnetic spiro isomer (Figure 1b) is more stable when the shortest center-to-periphery distance d of the vacancy is less than 7 Å (for definition of d, see Figure 1a). Creation of spiro isomers in the planes of graphene nanoribbons (GNRs) paves the way to achieving novel nanoarchitectures such as spiral helices.

[*] Dr. X. Gao, Prof. Dr. S. Nagase
Department of Theoretical and Computational Molecular Science
Institute for Molecular Science
Myodaiji, Okazaki 444-8585 (Japan)
Fax: (+81) 564-53-4660
E-mail: nagase@ims.ac.jp
L. Liu, Prof. Dr. S. Irle
Institute for Advanced Research and Department of Chemistry, Nagoya University
Nagoya 464-8602 (Japan)
Fax: (+81) 52-788-6151
E-mail: sirle@iar.nagoya-u.ac.jp

[**] This work was supported by a Grant-in-Aid for Scientific Research on Priority Area and Next Generation Super Computing Project (Nanoscience Program) from MEXT of Japan. L.L. is grateful for a GCOE PhD fellowship from the Department of Chemistry at Nagoya University, and S.I. acknowledges support by the Program for Improvement of Research Environment for Young Researchers from Special Coordination Funds for Promoting Science and Technology (SCF) commissioned by MEXT of Japan and by a Grant-in-Aid No. 20550012 from the Japan Society for the Promotion of Sciences (JSPS).

Supporting information for this article is available on the WWW under http://dx.doi.org/10.1002/anie.200907347.

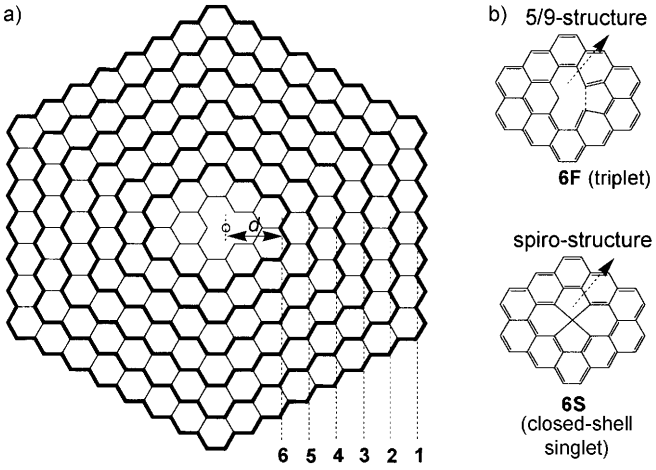

Figure 1. a) **1**–**6**: Hydrogen-terminated graphene flakes with monovacancies; the empty circle designates the vacant carbon position; d is the shortest center-to-periphery distance. b) **6F** and **6S**: Structures derived from **6** with 5/9 and spiro defects. Hydrogen atoms of all structures are omitted for clarity.

To investigate the low-lying structural and electronic conformation of graphene monovacancies, monovacant graphene flakes **1**–**6** with peripheries terminated by hydrogen atoms were used as model systems (Figure 1a). The largest flake, **1**, contains 351 carbon and 46 hydrogen atoms (Table 1). With decreasing molecular size from **1** to **6**, the d value decreases from 15.6 to 4.2 Å (Table 1). Thus, **1**–**6** provide reasonable models for monovacancy defects in graphenes with shrinking size and decreasing d. Geometry optimizations and energy calculations were performed by four methods: B3LYP/6-31G(d), GGA-PBE/DZP, and self-consistent-charge density functional tight binding with finite

Table 1: Shortest center-to-periphery distances d for graphene flakes **N** and the calculated energy differences [kcal mol^{-1}] between spiro and 5/9 defects ($E_{NS}-E_{NF}$) with various methods.[a]

N	d [Å]	$E_{NS}-E_{NF}$		
		GGA-PBE/DZP	B3LYP/6-31G(d)	DFTB[b]
1 ($C_{351}H_{46}$)	15.6	7.0[c]		9.0[c]
2 ($C_{265}H_{40}$)	12.8	6.1[c]		7.3[c]
3 ($C_{191}H_{34}$)	11.4	5.2[c]		4.7[c]
4 ($C_{129}H_{28}$)	8.5	0.6[c]	0.1[c]	0.7[c]
5 ($C_{79}H_{22}$)	7.1	−9.7[c]	−0.1[c]	−6.6[c]
6 ($C_{41}H_{16}$)	4.2	−26.2[c]	−12.7[c] (−9.3)[d]	−12.3[c]
7	4.2	−79.8[c]		

[a] For schematic structures of **1**–**6**, see Figure 1; for those of **7S** and **7F**, see Figure 2. [b] Energies and geometries of **NS** species were computed by DFTB with electronic temperature $T_e = 2000$ K, while SDFTB with $T_e = 0$ was used for **NF** species in their triplet electronic states. [c] Total energies without zero-point energies. [d] Gibbs free energies at 298.15 K.

electronic temperature (T_e) without and with inclusion of spin polarization (in the following denoted as DFTB and SDFTB, respectively). Although no spin polarization is included in the DFTB method, the finite electronic temperature allows an open-shell electronic structure to be effectively simulated in situations with near-degeneracy among the frontier orbitals.

For each monovacancy model (denoted as **N**, where **N** is **1**–**6**), our geometry optimization using the spin-polarized GGA-PBE/DZP method located a nearly planar 5/9 isomer **NF** having a total spin polarization ($Q_{up}-Q_{down}$) of 2. At the same time, geometry optimization with spin-unpolarized GGA-PBE/DZP located in every case a diamagnetic, nonplanar isomer **NS**, which corresponds to the spiro isomer without net spin (closed-shell singlet). The 5/9 isomers **NF** were computed with SDFTB by assuming a triplet electronic state, whereas the spiro isomers were well reproduced by spin-unpolarized DFTB. Table 1 lists the energy difference between each isomer pair ($E_{NS}-E_{NF}$). The GGA-PBE/DZP and (S)DFTB energies consistently show that the high-spin 5/9 isomers are more stable ($(E_{NS}-E_{NF})>0$) for larger models (i.e., **1**–**4**), whereas the nonmagnetic spiro isomers become more stable ($(E_{NS}-E_{NF})<0$) for smaller ones (i.e., **5** and **6**). For **4**–**6**, the same stability order was confirmed by the B3LYP calculations (Table 1). The possible existence of metastable spiro isomer in the side wall of carbon nanotubes has been mentioned before.[5] Similar spiro structures have also been reported in fused fullerenes.[6] However, the considerably higher thermodynamic stability we found for spiro isomers in **5** and **6** demonstrates for the first time that the spiro isomer is a stable defect derived from a monovacancy defect in graphene which has no radical character and differs substantially from the conventionally known 5/9 defects.

The presence of a spiro carbon center coils the graphene surface into a spiral helix with a dihedral angle of about 50° (e.g., see **6S** in Figure 2a). Consequently, the linear inclusion of four spiro carbon atoms in a GNR in a concerted manner results in a total dihedral angle of about 180° and hence

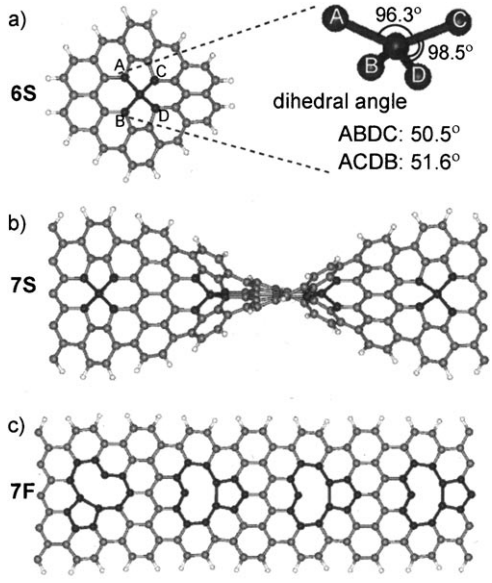

Figure 2. a) Optimized structure for **6S** [B3LYP/6-31G(d)]. b) and c) Optimized structures for GNR units **7S** and **7F** (GGA-PBE/DZP).

helical structure **7S** (Figure 2b). To compare the stabilities of 5/9 and spiro isomers in an infinite-length GNR, we optimized the structures and calculated the energies for **7S** and **7F** (Figure 2c), by using a periodical boundary condition at the GGA-PBE/DZP level. The results show that **7S** is nonmagnetic, whereas **7F** has an intrinsic magnetic moment. The calculated total energy for **7S** is lower than that of **7F** by 79.8 kcal mol^{-1} (Table 1). The markedly higher stability of **7S** relative to **7F** suggests that the spiro isomer is more stable than the 5/9 isomer, irrespective of the length of the ribbon. We note that **7S** shows a novel graphene-nanohelix structure, which suggests a fascinating role of spiro isomers in graphene-based architectural design.

The inclusion of a spiro isomer in the periphery of a graphene sheet should cause a smaller penalty of strain energy and thus higher stability than its inclusion in the interior of the graphene sheet. To demonstrate this point, besides **6S**, we located five other spiro isomers for **6**: **6SA**, **6SB**, **6SC**, **6SD** and **6SE** (Figure 3). Isomers **6SD** and **6SE** have spiro isomers much closer to the periphery than **6S**. As shown in Figure 3, the calculated relative Gibbs free energies for **6SD** (−102.2 kcal mol^{-1}) and **6SE** (−145.4 kcal mol^{-1}) are indeed much lower than that for **6S** (−9.3 kcal mol^{-1}). The outstanding stabilities of **6SD** and **6SE** over **6S** indicate that the distance to the periphery (i.e. d as defined in Figure 1a) is the factor dominating the preference between 5/9 and spiro isomers of graphene monovacancies. Figure 3 also shows the reaction-energy profile for the transformation of **6S** into **6SE**. The Gibbs free energy of activation $G^{\neq}$ for the rate-determining step, that is, from **6S** to **6SA**, is 17.8 kcal mol^{-1} (Figure 3). This activation energy indicates that the spiro isomer **6S** has considerable stability at a relatively low temperature. However, **6S** is subject to transformation into **6SE** at high temperature. To demonstrate this, we performed quantum chemical molecular dynamics (QM/MD) simulations based on the DFTB method. The velocity Verlet algorithm was used for time integration, facilitating a time step Δt of 0.2 fs, while the temperature was controlled by using an Andersen thermostat with a reselect probability of 0.2. Using the geometry **6S** as model system, we first equilibrated the structure at a nuclear temperature $T_n=$ 1000 K for 10 ps. From this equilibration run, we extracted ten geometry snapshots, which were then propagated at $T_n=$ 2000 K for 1 ns. Indeed, taking **6S** as the initial structure, our QM/MD simulation of thermal annealing at a nuclear temperature $T_n=1000$ K for 10 ps showed that the structure only oscillates randomly about the equilibrium geometry of **6S** (Figure S2 of Supporting Information). In contrast, in the simulation with **ts1** (see Figure S3a of Supporting Information) as initial structure at a nuclear temperature $T_n=2000$ K, chemical transformations of Figure 3 were observed. For example, the structure similar to **6S** (Figure S3b, Supporting Information) appears at 12.97 ps. This structure transforms into the structure similar to **6SA** (Figure S3d, Supporting Information) at 23.30 ps, via the structure similar to **ts1** (Figure S3c, Supporting Information). At 299.15 ps, the structure similar to **6SC** (Figure S3e, Supporting Information) appears. The structure similar to **6SD** is formed via a structure resembling **ts4** (Figure S3f, Supporting Information). At

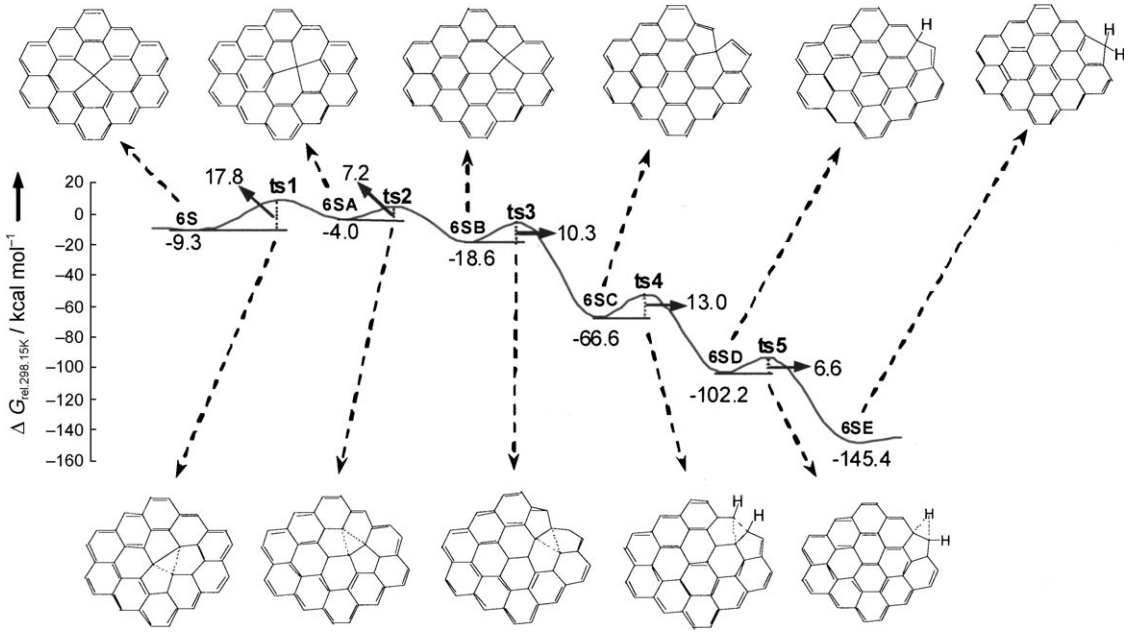

Figure 3. Reaction-energy profile for the structural transformation of **6S** into **6SE**. Gibbs free energies with respect to **6F** for the intermediates and Gibbs free-energies of activation for the transition states are indicated [B3LYP/6-31G(d)]. For each transition state, the left dashed line designates the breaking bond, and the right one the forming bond. Hydrogen atoms are omitted, except for those close to the reaction centers.

600.00 ps, the structure similar to **6SE** appears, and dominates the subsequent trajectories. These results suggest that high-temperature thermal annealing will serve as an efficient approach to remove unwanted spiro defects from graphene. The predicted considerable thermal stability of spiro isomer at the periphery of graphene indicates its existence at graphene peripheries at room temperature. This is in good agreement with the curvatures that have been observed experimentally along the peripheries of defective graphenes.[2f]

In conclusion, the stable configuration of graphene monovacancy is determined by its location in the graphene sheet. A nearly planar 5/9 isomer is the stable conformation for interior monovacancies, whereas a nonplanar spiro isomer is the most stable structure for monovacancies close to the periphery ($d < 7$ Å). Unlike the magnetic 5/9 isomer, the spiro isomer does not contribute any unpaired electrons. On thermal annealing, the spiro isomer is subject to migrating towards the outmost periphery of graphene. Therefore, high-temperature thermal annealing can serve as an efficient approach for the elimination of undesirable spiro defects from graphene. Thanks to its associated dihedral angles and considerable room-temperature stability, the spiro isomer provides an ideal structural building unit that coils graphene surfaces into spiral helices. These results predict a family of novel carbon architectures that can be derived from graphene monovacancies.

Received: December 30, 2009
Published online: March 23, 2010

Keywords: carbon · density functional calculations · electronic structure · helical structures · molecular dynamics

[1] a) K. S. Novoselov, A. K. Geim, S. V. Morozov, D. Jiang, Y. Zhang, S. V. Dubonos, I. V. Grigorieva, A. A. Firsov, *Science* **2004**, *306*, 666; b) K. Müllen, J. P. Rabe, *Acc. Chem. Res.* **2008**, *41*, 511, and references therein; c) S. Park, R. S. Ruoff, *Nat. Nanotechnol.* **2009**, *4*, 217, and references therein.

[2] a) P. Esquinazi, D. Spemann, R. Höhne, A. Setzer, K. H. Han, T. Butz, *Phys. Rev. Lett.* **2003**, *91*, 227201; b) P. Ruffieux, O. Gröning, P. Schwaller, L. Schlapbach, P. Gröning, *Phys. Rev. Lett.* **2000**, *84*, 4910; c) J. C. Meyer, C. Kisielowski, R. Erni, M. D. Rossell, M. F. Crommie, A. Zettl, *Nano Lett.* **2008**, *8*, 3582; d) A. Hashimoto, K. Suenaga, A. Gloter, K. Urita, S. Iijima, *Nature* **2004**, *430*, 870; e) J. Coraux, A. T. N'Diaye, C. Busse, T. Michely, *Nano Lett.* **2008**, *8*, 565; f) M. H. Gass, U. Bangert, A. L. Bleloch, P. Wang, R. R. Nair, A. K. Geim, *Nat. Nanotechnol.* **2008**, *3*, 676.

[3] a) R. H. Telling, C. P. Ewels, A. A. El-Barbary, M. I. Heggie, *Nat. Mater.* **2003**, *2*, 333; b) D. W. Boukhvalov, M. I. Katsnelson, *Nano Lett.* **2008**, *8*, 4373; c) H. Ohldag, T. Tyliszczak, R. Höhne, D. Spemann, P. Esquinazi, M. Ungureanu, T. Butz, *Phys. Rev. Lett.* **2007**, *98*, 187204; d) K. H. Han, D. Spemann, P. Esquinazi, R. Höhne, V. Riede, T. Butz, *Adv. Mater.* **2003**, *15*, 1719; e) C. D. Latham, M. I. Heggie, J. A. Gámez, I. Suárez-Martínez, C. P. Ewels, P. R. Briddon, *J. Phys. Condens. Matter* **2008**, *20*, 395220; f) I. Suarez-Martinez, G. Savini, G. Haffenden, J.-M. Campanera, M. I. Heggie, *Phys. Status Solidi C* **2007**, *4*, 2958; g) For a review, see: R. H. Telling, M. I. Heggie, *Philos. Mag.* **2007**, *87*, 4797.

[4] a) A. A. El-Barbary, R. H. Telling, C. P. Ewels, M. I. Heggie, P. R. Briddon, *Phys. Rev. B* **2003**, *68*, 144107; b) P. O. Lehtinen, A. S. Foster, Y. Ma, A. V. Krasheninnikov, R. M. Nieminen, *Phys. Rev. Lett.* **2004**, *93*, 187202; c) Y. Ma, P. O. Lehtinen, A. S. Foster, R. M. Nieminen, *New J. Phys.* **2004**, *6*, 68; d) H. Kumazaki, D. S. Hirashima, *J. Phys. Soc. Jpn.* **2007**, *76*, 064713; e) O. V. Yazyev, L. Helm, *Phys. Rev. B* **2007**, *75*, 125408; f) J. J. Palacios, J. Fernández-Rossier, L. Brey, *Phys. Rev. B* **2008**, *77*, 195428; g) O. V. Yazyev, *Phys. Rev. Lett.* **2008**, *101*, 037203; h) R. Singh, P. Kroll, *J. Phys. Condens. Matter* **2009**, *21*, 196002; i) H. Tachikawa, H. Kawabata, *J. Phys. Chem. C* **2009**, *113*, 7603.

[5] S. Berber, A. Oshiyama, *Physica B* **2006**, *376–377*, 272.

[6] T. Heine, F. Zerbetto, G. Seifert, P. W. Fowler, *J. Phys. Chem. A* **2000**, *104*, 3865.

